Research Article

Emile F. Doungmo Goufo* and Amos Kubeka

Accumulation process in the environment for a generalized mass transport system

https://doi.org/10.1515/phys-2024-0054
received April 16, 2024; accepted June 18, 2024

Abstract: In last decades, there have been drastic environmental transformations and mutations happening all around the world. Due to the continuous mass transfer process, for example, CO_2 mass transfer, which in this case, takes the form of greenhouse gas emissions, unusual and extreme kinds of phenomena have been occurring here and there, disturbing our ecosystems and causing damage and chaos on their paths. Reducing or stopping these gas emissions has become one of the major topics in our planet. We investigate the solvability of a mathematical model describing the mass transport process in nature and where additional perturbations parameters have been considered. Besides addressing the stability of the model, its convergence analysis is also given with the use of Crank–Nicholson numerical method, in order to assess its efficiency and perform some numerical simulations. The results obtained show that the model's dynamic is characterized by many grouping (accumulation) zones, where mass (of CO_2, for instance) accumulates in an increasing way. This result is important in controlling how CO_2 can be stored in this growingly perturbed environment that surrounds us.

Keywords: mass transport, CO_2 emission process, fractional time order derivative, stability and convergence analysis

1 Introduction and basic concepts

The heat or mass transfer dynamics can be observed in many areas and aspects of real life. Particularly, when physical material that exists in a homogenous phase is transported to another homogenous phase. The main distinction between the two phases involved in the transfer process is the difference of state (diffusivity, solubility). As a simple example for mass transfer, we have a system of gas–liquid contact (Figure 1) where, for instance, the marine or freshwater that was previously left on the ground will certainly evaporate as the result of water molecules (H_2O) that diffuse into the air [1]. Such evaporation has proven to be intense during the last decades, and the water cycle is severely impacted by the climate change causing drought and drying up of waterways. Another example for mass transfer occurs in a complex geological system (Figure 2) where carbon dioxide (CO_2) molecules (or mass) are transported and deeply stored below the earth surface [2]. Mass transfer also plays an important role in soil restoration where processes such as evaporation and condensation are the main key and driving factors. The dynamic characterizing the heat transfer is similar to the one that characterizes the mass transfer and both transfers can happen simultaneously since heat transfer usually results from the mass difference between two interacting objects. Skočilasová *et al.* [3] analyzed a particular case of heat transfer occurring inside a pipe and involving a fluid and a turbulent flow regiment.

Therefore, the process of mass or heat transfer depicts the mass transportation or heat diffusion from a particular area to another and is one of the pioneer concepts that lie at the core of the transport theory. It is important to recall that describing the way mass is transported from one point/region to another is one of the major purposes of the mass transfer equation, making such an equation unavoidable in the area of transport theory. The process of mass transfer can happen either in one phase or in multiple phases involving phase boundaries. The most common case widely used in science problems is the one where least one fluid phase is involved in the mass transfer process. These fluid phases are commonly liquid or gas. Solid phase can also be described as well. In the sense of general analysis, the mass transfer equation can take the form [4]:

$$\varepsilon\beta[M_t(t,x) + \theta u M_x(t,x)] = \kappa M_{xx}(t,x) + \mathbb{S}(t,x).$$

An equivalent version is

*** Corresponding author: Emile F. Doungmo Goufo,** Mathematical Sciences, University of South Africa, Florida 0003, South Africa, e-mail: franckemile2006@yahoo.ca
Amos Kubeka: Mathematical Sciences, University of South Africa, Florida 0003, South Africa

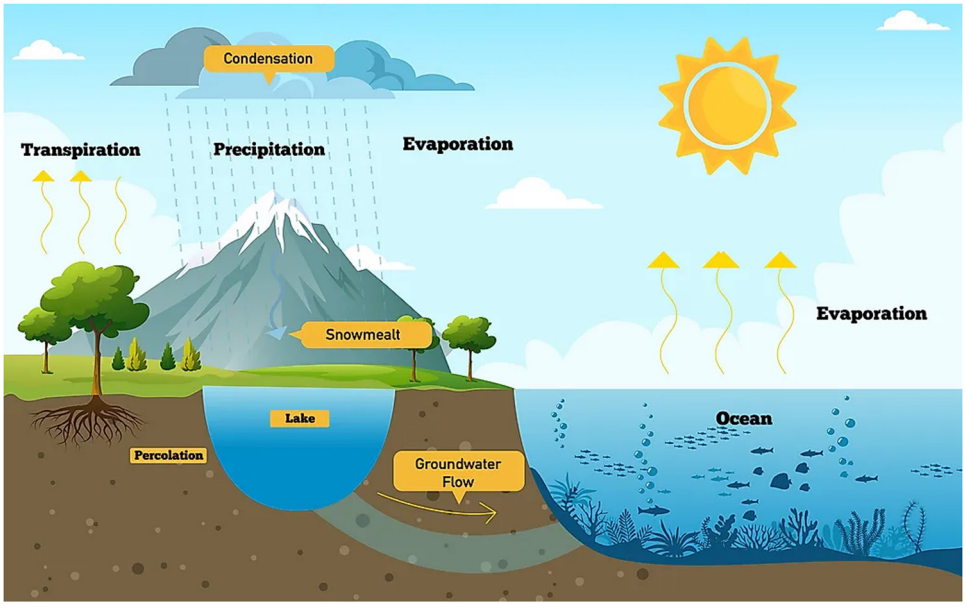

Figure 1: Gas–liquid contact involved in the process of mass transfer (evaporation) and where, for instance, water cycle can be severely impacted by the climate change [1].

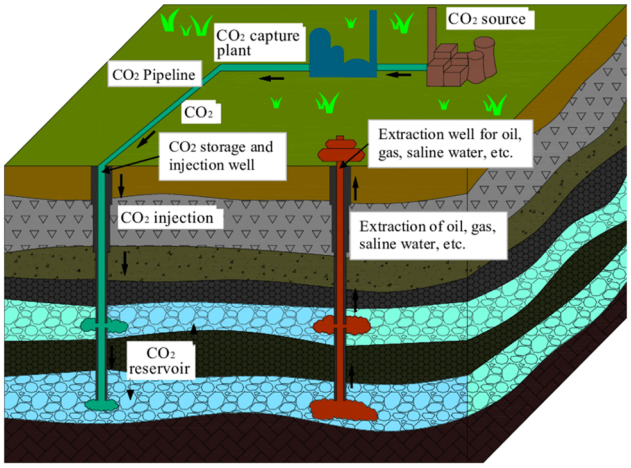

Figure 2: Complex geological system showing how molecules of carbon dioxide (CO_2), for instance, can be transported and deeply stored below the earth surface [2].

$$M_t(t,x) = -\theta u M_x(t,x) + \nu M_{xx}(t,x) + \frac{1}{\varepsilon\beta}\mathbb{S}(t,x), \qquad (1)$$

where $M_t = \frac{\partial M}{\partial t}$, $M_{xx} = \frac{\partial^2 M}{\partial x^2}$, and $\nu = \frac{\kappa}{\varepsilon\beta}$ with t representing the time variable and x the spatial variable. The dependent variable M represents the mass concentration, u the velocity, θ the porosity, ε the density of mass, κ the thermal conductivity, β the specific heat, and finally $\mathbb{S}$ the source term. Recall that the basic principle that generated this mass transfer equation can be compared with its analogy with the mathematical equation in the heat transfer, which considerably depends on the temperature difference driving force for heat flow. Hence, the mass can be calculated using the specific heat capacity taking the form $M = \frac{q}{\Delta T \cdot C}$, where q is the heat transferred, ΔT is the change in temperature, and C is the specific heat capacity.

There exist in the literature different techniques used for the derivation and generation of mass or heat transfer equations. In the process of generation, their theoretical significance in real life and their relation to other theories such as the general diffusion theory are given. For the reader interested in the methods used to establish general mass/heat transfer equations, we refer the articles [4–6] and also references therein.

Using the values given in Table 1 for the parameters involved in Eq. (1), we can generate its numerical representation as the one shown in Figure 3 and which depicts the spatial evolutive dynamics of the mass involved in the transfer process within the x-space interval $[0, 40]$ as time t varies from 0 to 20. The figure shows only one major mass

Table 1: Parameters' estimation

Description (parameters' symbols)	Estimated values
Mass density (ε)	0,05 (kg)
Porosity (θ)	0.005 (–)
Thermal conductivity (κ)	10 (W K^{-1} m^{-1})
$\nu = \frac{\kappa}{\varepsilon\beta}$	~0,9
Specific heat (β)	~222 (J kg^{-1} K^{-1})
Velocity (u)	~20 (m s^{-1})
Source term ($\mathbb{S}$)	0,2 (W m^{-3})

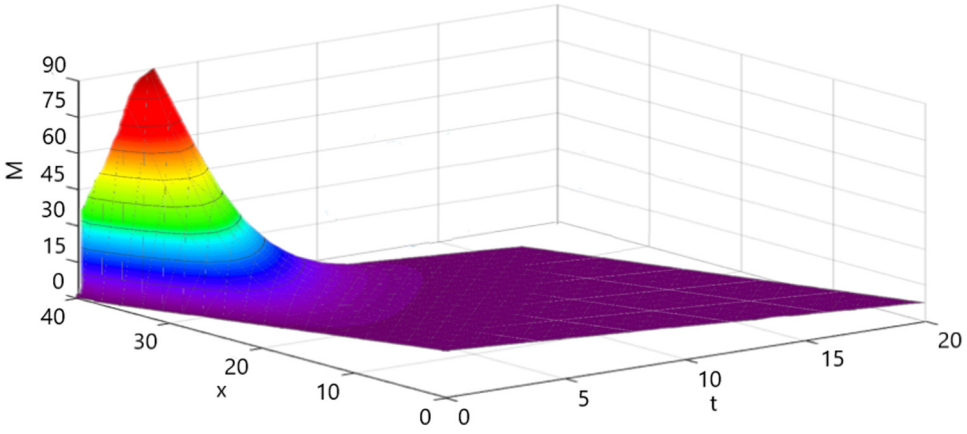

Figure 3: The spatial evolutive dynamics of the mass involved in the transfer process within the x-space interval $[0, 40]$ as time t varies from 0 to 20. It shows only one major mass grouping arising mostly in the interval $30 \le x \le 40$, for $t \in [0, 4]$. There is a relatively uniform and flat evolution elsewhere in the space.

cluster arising mostly in the interval $30 \le x \le 40$ and a relatively constant and flat evolution elsewhere in the space.

Now, the question that presents itself is whether there is a way of creating a variety of mass clustering across different scales in the evolutive system. We try to give an answer by investigating the perturbed version of the equation where some model's parameters and terms have been added. The Caputo–Fabrizio operator [7] is one of the perturbing factors to be considered.

After defining the Caputo–Fabrizio operator in Section 2, we describe succinctly the Crank–Nicholson numerical scheme, before continuing in Section 2.1 where we show the stability result of the scheme. In Section 2.2, we proceed by showing the convergence result of the scheme before ending in Section 2.3 where numerical representations are performed. Finally, we conclude the whole analysis by clearly expressing the main results of this article.

2 Numerical solvability of the mass transfer model

Let us recall the fractional operator that was proposed in order to depict particular behavior that occurs in multiscale systems and materials with massive heterogeneities. It is called the Caputo–Fabrizio fractional derivative, and was proposed by authors of the same names [7]. Today considered as the derivative of fractional order with no singular kernel, it is expressed by:

Definition 2.1. (Caputo–Fabrizio derivative) Let us assume that the function M is taken from $H^1(0;b)$; $b > 0$; $\varrho \in [0; 1]$, then its Caputo–Fabrizio fractional derivative of order ϱ reads as:

$$ {}^{cf}D_t^{\varrho}M(t) = \frac{\alpha}{(1-\varrho)}\int_0^t \dot{M}(\eta)\exp\left(-\frac{\varrho(t-\eta)}{1-\varrho}\right)\mathrm{d}\eta. \tag{2}$$

However, if we assume that the function M is not taken from $H^1(0; b)$; $b > 0$, then, its Caputo–Fabrizio fractional derivative of order ϱ reads as:

$$ {}^{cf}D_t^{\varrho}M(t) = \frac{\varrho\alpha}{(1-\varrho)}\int_0^t (M(t)-M(\eta))\exp\left(-\frac{\varrho(t-\eta)}{1-\varrho}\right)\mathrm{d}\eta, \tag{3}$$

where α is a real constant. Losada and Nieto [8] upgraded this definition of Caputo–Fabrizio fractional derivative as follows:

$$ {}^{cf}D_t^{\varrho}M(t) = \frac{(2-\varrho)}{2(1-\varrho)}\int_0^t \dot{M}(\eta)\exp\left(-\frac{\varrho(t-\eta)}{1-\varrho}\right)\mathrm{d}\eta. \tag{4}$$

Now, using the Caputo–Fabrizio derivative, Model (1) is modified and expressed as

$$\begin{aligned} {}^{cf}D_t^{\varrho}M(t,x) = &-\theta u\frac{\partial M}{\partial x}(t,x) + \nu\frac{\partial^2 M}{\partial x^2}(t,x) \\ &+ \frac{1}{\varepsilon\beta}\mathbb{S}(t,x), \quad t \ge 0, \end{aligned} \tag{5}$$

satisfying the initial condition

$$M(0,x) = \phi(x), \tag{6}$$

as well as the boundary conditions

$$M(t,0) = \frac{t}{3} \quad \text{and} \quad M(t,\mathbf{L}) = \frac{\cosh t}{3}. \tag{7}$$

Recall that the variable x represents the spatial component, t represents the time component with M, θ, and u, respectively, representing the mass concentration, the porosity, and the velocity. Mass density is given by ε, the specific heat given by β, the thermal conductivity represented by κ, the source term given by $\mathbb{S}$, and finally, $\nu = \frac{\kappa}{\varepsilon\beta}$.

In the last decades, a number of research and publications have analyzed mathematical models describing dynamical processes such as dispersion, advection, and also diffusion. Innovative methods and techniques involving fractional calculus (fixed or variable derivative order) were used in many research publications [9–12]. For instance, Atangana [9] used the concept to analyze the stability and convergence results of the time-fractional variable order telegraph equation. For instance, Lin *et al.* [10] proposed an explicit numerical scheme able to easily approximate the problems under study. Another specific example is found in Goufo [12] where they applied the concept on an epidemic model to analyze the stability of the Ebola hemorrhagic fever dynamics with a nonlinear transmission. Fractional models with constant order's derivative particularly sparked many studies [13–17]. For example, technique like implicit difference was used and proven to be a useful tool in solving time-dependent diffusion equation [13] or technique like weighted average finite difference proven in the study of Yuste *et al.* [18] to be a valuable tool for solving the same type of diffusion differential systems. Other valuable techniques are described in previous articles [19–21], some of them using matrix analysis and flexible numerical scheme have proven to be efficient for solving fractional models where the main variables change in both space and time. Let us now describe the numerical scheme considered here to be the most suitable for the study, analysis and solvability of Systems (5)–(7); it is based on the Crank–Nicholson numerical scheme as proposed in the study of Diethelm *et al.* [21].

Using the discretization

$$t_p = pv, \quad \text{with } 0 \le p \le \mathbf{n}, \quad \mathbf{n}v = \mathbf{T}, \quad \text{and}$$
$$x_b = ba, \quad \text{with } 0 \le b \le \mathbf{m}, \quad \mathbf{m}a = \mathbf{L},$$

where $\mathbf{n}$ and $\mathbf{m}$ are the numbers of grid points and a the step size. Using Crank–Nicholson-related discretization, the explicit formula for the first-order derivative with respect to the x-component can be expressed by

$$\frac{\partial M}{\partial x} = \frac{1}{2}\left\{\frac{M(t_{p+1}, x_{b+1}) - M(t_{p+1}, x_{b-1})}{2a} + \frac{M(t_p, x_{b+1}) - M(t_p, x_{b-1})}{2a}\right\} + O(a). \tag{8}$$

Moreover,

$$M = \frac{1}{2}(M(t_{p+1}, x_b) + M(t_p, x_b)). \tag{9}$$

By Crank–Nicholson time discretizing, the explicit formula for the derivative of order one with respect to the t-variable can be expressed by

$$\frac{\partial M}{\partial t} = \frac{1}{2}\left\{\frac{M(t_{p+1}, x_{b+1}) - M(t_{p+1}, x_{b-1})}{2v} + \frac{M(t_p, x_{b+1}) - M(t_p, x_{b-1})}{2v}\right\} + O(v). \tag{10}$$

Similarly, the explicit formula for the derivative of order two with respect to the time t can be expressed by

$$\frac{\partial^2 M}{\partial t^2} = \frac{1}{2}\left\{\frac{M(t_{p+1}, x_{b+1}) - 2M(t_p, x_{b+1}) + M(t_{p-1}, x_{b+1})}{v^2} + \frac{M(t_{p+1}, x_b) - 2M(t_p, x_b) + M(t_{p-1}, x_b)}{v^2}\right\} + O(v^2). \tag{11}$$

Discretizing the Caputo–Fabrizio derivative *via* Crank–Nicholson approach at a point (t_p, x_b) gives the explicit formula:

$${}^{cf}D_t^{\varrho} M(t_p, x_b) = \frac{\alpha}{1-\varrho}\left[\sum_{j=1}^{p-1}\left\{\frac{M(t_{p-j-1}, x_b) - M(t_{p-j}, x_b)}{\eta}\right\}\mathbf{q}_j^{p+1} + M(t_{p+1}, x_b) - M(t_p, x_b)\right] + O(\eta^2), \tag{12}$$

with the coefficients expressed as

$$\mathbf{q}_j^{p+1} = \exp\left\{\frac{-\varrho\eta}{1-\varrho}(p-j)\right\} - \exp\left\{\frac{-\varrho\eta}{1-\varrho}(p-j+1)\right\}, \quad j = 1, \cdots, p+1. \tag{13}$$

We can now substitute (8)–(12) into (5) and obtain

$$\begin{aligned}
&\frac{\alpha}{1-\varrho}\left[\sum_{j=1}^{p-1}\left\{\frac{M(t_{p-j-1}, x_b) - M(t_{p-j}, x_b)}{\eta}\right\}\mathbf{q}_j^{p+1} + M(t_{p+1}, x_b) - M(t_p, x_b)\right] \\
&+ \theta u\frac{1}{2}\left\{\frac{M(t_{p+1}, x_{b+1}) - M(t_{p+1}, x_{b-1})}{2a} + \frac{M(t_p, x_{b+1}) - M(t_p, x_{b-1})}{2a}\right\} \\
&- \nu\kappa\frac{1}{2}\left\{\frac{M(t_{p+1}, x_{b+1}) - 2M(t_{p+1}, x_b) + M(t_{p+1}, x_{b-1})}{a^2} + \frac{M(t_p, x_{b+1}) - 2M(t_p, x_b) + M(t_p, x_{b-1})}{a^2}\right\} \\
&- \frac{1}{2\varepsilon\beta}(\mathbb{S}(t_{p+1}, x_b) + \mathbb{S}(t_p, x_b)) = 0.
\end{aligned} \tag{14}$$

Using the following simplified notations

$$M^{b,p} = M(t_p, x_b), \quad \mathbb{S}^{b,p} = \mathbb{S}(t_p, x_b),$$

$$\lambda_{\varrho} = \frac{\theta u \varrho[\alpha]^{-1}}{4a}, \quad \zeta_{\varrho} = \frac{\nu\kappa\varrho[\alpha]^{-1}}{2a^2},$$

$$\varpi^{b,p} = \frac{\varrho[\alpha]^{-1}\mathbb{S}^{b,p}}{2\varepsilon\beta},$$

$$\mathbf{E}_j^{b,p+1} = \mathbf{q}_{j-1}^{p+1} - \mathbf{q}_j^{p+1} \quad \text{with } \mathbf{E}_0^{b,p+1} = 1, \tag{15}$$

reduces the equality (14) to

$$\begin{aligned} M^{b,p+1} - M^{b,p} + \sum_{j=1}^{p}[M^{b,p+1-j} - M^{b,p-j}]\mathbf{q}_j^{p+1} \\ = -\lambda_{\varrho}(M^{b+1,p+1} - M^{b-1,p+1} + M^{b+1,p} - M^{b-1,p}) \\ + \zeta_{\varrho}(M^{b+1,p+1} - M^{b,p+1} - (M^{b,p+1} - M^{b-1,p+1})) \\ + \zeta_{\varrho}(M^{b+1,p} - M^{b,p} - (M^{b,p} - M^{b-1,p})) \\ + \varpi^{b,p}(\mathbb{S}^{b,p+1} + \mathbb{S}^{b,p}). \end{aligned} \tag{16}$$

Re-arranging (16) leads to

$$\begin{aligned} M^{b,p+1}[1 + 2\zeta_{\varrho}] \\ = M^{b,p}[1 - 2\zeta_{\varrho}] - \lambda_{\varrho}(M^{b+1,p+1} - M^{b-1,p+1} + M^{b+1,p} \\ - M^{b-1,p}) + \zeta_{\varrho}(M^{b+1,p+1} + M^{b-1,p+1} + M^{b+1,p} + M^{b-1,p}) \\ + \varpi^{b,p}(\mathbb{S}^{b,p+1} + \mathbb{S}^{b,p}) + \sum_{j=1}^{p}[M^{b,p+1-j} - M^{b,p-j}]\mathbf{q}_j^{p+1}. \end{aligned} \tag{17}$$

It is now time to analyze the stability of the mass transfer model *via* (17).

2.1 Stability analysis of the mass transfer dynamic

Based on the aforementioned notations, definitions, and setting, we can state the following proposition.

Proposition 2.1. *The approximation scheme based on the Crank–Nicholson approach described in* Section 2 *and used to approximate the solution for the mass transfer system* (5) *is stable.*

Proof. We start the proof by considering the approximation $\mathbf{I}^{b,p} = \mathbf{I}(t_p, x_b)$ at the point (t_p, x_b), $b = 1, 2, \ldots, \mathbf{m} - 1$, $p = 1, 2, \ldots, \mathbf{n}$.

Let us define $\mathbf{k}^{b,p} = M^{b,p} - \mathbf{I}^{b,p}$ and $\mathbf{k}^{p} = [\mathbf{k}^{1,p}, \mathbf{k}^{2,p}, \ldots, \mathbf{k}^{\mathbf{m}-1,p}]^{\mathbf{T}}$, which satisfies

$$\mathbf{k}^{p}(x) = \begin{cases} \mathbf{k}^{b,p}, & \text{for } x_b - a/2 < x < x_b + a/2, \\ 0, & \text{for } \mathbf{L} - a/2 < x \le \mathbf{L}. \end{cases} \tag{18}$$

It appears that the function $\mathbf{k}^{p}(x)$ is expandable into the Fourier series to become

$$\mathbf{k}^{p}(x) = \sum_{\bar{j}=-\infty}^{+\infty} \delta_{\bar{j}}(\bar{j}) e^{i2\pi\bar{j}\,p/\mathbf{L}} \tag{19}$$

with δ the Dirac Delta operator. To support the proof and explain some of it steps, we need to state the following assertions and properties that are related to the the model's parameters.

Remark 2.1.

- $1 > 1 - \varrho_b^{p+1} \ge 0$, for all $b, p > 0$.
- $1 \ge \mathbf{q}_j^{p+1} \ge 0$, for all $p = 1, 2, \ldots, \mathbf{n}$.
- $\sum_{j=0}^{p-1}\mathbf{q}_{j+1}^{p+1} = 1 - \mathbf{E}_p^{b,p+1}$, for $b = 1, 2, \ldots, \mathbf{m} - 1$.
- $1 \ge \mathbf{E}_{j-1}^{b,p} \ge \mathbf{E}_j^{b,p} > 0$, $1 \le j \le p$.
- The coefficients λ_{ϱ}, ζ_{ϱ}, and $\varpi_j^{b,p}$ are non-negative for all $b = 1, 2, \ldots, \mathbf{m} - 1$.

Hence, adopting the Crank–Nicholson numerical method to solve the mass transfer model causes an absolute error given by the following relation:

$$\begin{aligned} \mathbf{k}^{b,p+1}[1 + 2\zeta^{b,p+1}] \\ = \mathbf{k}^{b,p}[1 - 2\zeta^{b,p+1}] \\ - \lambda^{b,p+1}(\mathbf{k}^{b+1,p+1} - \mathbf{k}^{b-1,p+1} + \mathbf{k}^{b+1,p} - \mathbf{k}^{b-1,p}) \\ + \zeta^{b,p+1}(\mathbf{k}^{b+1,p+1} + \mathbf{k}^{b-1,p+1} + \mathbf{k}^{b+1,p} + \mathbf{k}^{b-1,p}) \\ + \varpi^{b,p}(\mathbb{S}^{b,p+1} + \mathbb{S}^{b,p}) + \sum_{j=1}^{p}[\mathbf{k}^{b,p+1-j} - \mathbf{k}^{b,p-j}]\mathbf{q}_j^{b,p+1}. \end{aligned} \tag{20}$$

In addition, if it is assumed that the error function $\mathbf{k}^{b,p}$ can take the expression of the Dirac Delta-exponential function

$$\mathbf{k}^{b,p} = \delta_p e^{i\varsigma pb}, \tag{21}$$

where ς represents the real spatial wave, then induction on p and additional development lead to

$$
\begin{aligned}
|\delta_{p+1}| &\le \left[\frac{\left|1-\sqrt{2}\sin^2\left(\frac{\varsigma a}{3}\right)\lambda^{b,p+1}-2(\varpi_j^{b,p}(\mathbb{S}^{b,p+1}+\mathbb{S}^{b,p}))\sin^2\left(\frac{\varsigma a}{3}\right)\right|}{\left|1+\sqrt{2}\sin^2\left(\frac{\varsigma a}{3}\right)\lambda^{b,p+1}+2(\varpi_j^{b,p}(\mathbb{S}^{b,p+1}+\mathbb{S}^{b,p}))\sin^2\left(\frac{\varsigma a}{3}\right)\right|}\right]\delta_0,\\
&= \left[\frac{\left|1-\sqrt{2}\sin^2\left(\frac{\varsigma a}{3}\right)\lambda^{b,p+1}-2(\varpi_j^{b,p}(\mathbb{S}^{b,p+1}+\mathbb{S}^{b,p}))\sin^2\left(\frac{\varsigma a}{3}\right)\right|}{\left|1+\sqrt{2}\sin^2\left(\frac{\varsigma a}{3}\right)\lambda^{b,p+1}+2(\varpi_j^{b,p}(\mathbb{S}^{b,p+1}+\mathbb{S}^{b,p}))\sin^2\left(\frac{\varsigma a}{3}\right)\right|}\right]|\delta_0|,\\
&\le \left[\frac{\left|1+\sqrt{2}\sin^2\left(\frac{\varsigma a}{3}\right)\lambda^{b,p+1}+2(\varpi_j^{b,p}(\mathbb{S}^{b,p+1}+\mathbb{S}^{b,p}))\sin^2\left(\frac{\varsigma a}{3}\right)\right|}{\left|1+\sqrt{2}\sin^2\left(\frac{\varsigma a}{3}\right)\lambda^{b,p+1}+2(\varpi_j^{b,p}(\mathbb{S}^{b,p+1}+\mathbb{S}^{b,p}))\sin^2\left(\frac{\varsigma a}{3}\right)\right|}\right]|\delta_0|,\\
&= |\delta_0|,
\end{aligned}
\tag{22}
$$

which concludes the proof for the stability result. □

2.2 Convergence analysis of the mass transfer dynamic

We continue in this section our analysis by completing the solvability of the mass transfer Systems (5)–(7). For that, we investigate the convergence state of the system in connection to the Crank–Nicholson scheme presented in the previous sections. It is important to point out the existence of real constants $\gamma_1, \gamma_2, \gamma_3, \gamma_4, \gamma_5 > 0$ so that the following approximations, related to equations (8) to (11) are possible and read as

$$
\frac{\partial M}{\partial x} + M\gamma_1 = \frac{1}{2}\left(\frac{M(t_{p+1}, x_{b+1}) - M(t_{p+1}, x_{b-1})}{2a} + \frac{M(t_p, x_{b+1}) - M(t_p, x_{b-1})}{2a}\right), \tag{23}
$$

$$
\frac{\partial M}{\partial t} + v\gamma_3 = \frac{1}{2}\left(\frac{M(t_{p+1}, x_{b+1}) - M(t_{p+1}, x_{b-1})}{2v} + \frac{M(t_p, x_{b+1}) - M(t_p, x_{b-1})}{2v}\right), \tag{24}
$$

$$
\begin{aligned}
&\frac{\partial^2 M}{\partial t^2} + v^2\gamma_4\\
&= \frac{1}{2}\left(\frac{M(t_{p+1}, x_{b+1}) - 2M(t_p, x_{b+1}) + M(t_{p-1}, x_{b+1})}{v^2} + \frac{M(t_{p+1}, x_b) - 2M(t_p, x_b) + M(t_{p-1}, x_b)}{v^2}\right),
\end{aligned}
\tag{25}
$$

$$
\begin{aligned}
&{}^{cf}D_t^{\varrho}M(t_p, x_b) + v\gamma_5\\
&= \frac{a}{\varrho}\left[\sum_{j=1}^{p-1}\left(\frac{M(t_{p-j-1}, x_b) - M(t_{p-j}, x_b)}{\eta}\right)\mathbf{q}_j^{p+1} + M(t_{p+1}, x_b) - M(t_p, x_b)\right].
\end{aligned}
\tag{26}
$$

Then, choosing $M(t_p, x_b)$, $b = 1, 2, \ldots, \mathbf{m}$, $p = 1, 2, \ldots, \mathbf{n} - 1$, to be the exact solution, at the point (t_p, x_b), of the Cauchy problem associated to the mass transfer system, we can pose $\Psi^{b,p} = M(t_p, x_b) - x^{b,p}$, and $\Psi^p = [\Psi^{0,p} = 0, \Psi^{1,p}, \Psi^{2,p}, \ldots, \Psi^{\mathbf{m}-1,p}]^{\mathrm{T}}$. Therefore, (20) is equivalent for $p = 0$, to

$$
\begin{aligned}
&\Psi^{b,1}[1 + \zeta^{b,1}(\Psi_j^{b,1})(\mathbb{S}^{b,1} + \mathbb{S}^{b,0})]\\
&\quad - (\Psi^{b+1,1} - \Psi^{b-1,1})\lambda^{b,1} + \varpi_j^{b,0}(\Psi_j^{b,1})(\mathbb{S}^{b,1} + \mathbb{S}^{b,0})\\
&\quad = \Pi^{b,1},
\end{aligned}
\tag{27}
$$

$1 \le j \le p$ and for $p > 0$, to

$$
\begin{aligned}
&\Psi^{b,p+1}[1 + \zeta_{\varrho}(\mathbb{S}^{b,p+1} + \mathbb{S}^{b,p})(\Psi_j^{b,p+1} + \Psi_j^{b,p})]\\
&\quad - (\Psi^{b+1,p+1} - \Psi^{b-1,p+1})\lambda_{\varrho} + \sum_{j=1}^{p}[\Psi^{b,p+1-j} + \Psi^{b,p-j}]\mathbf{q}_j^{p+1}\\
&\quad + \varpi_j^{b,p}(\mathbb{S}^{b,p+1} + \mathbb{S}^{b,p})(\Psi_j^{b,p+1}) = \Pi^{b,p+1},
\end{aligned}
\tag{28}
$$

$1 \le j \le p$. Recall that the quantity $\Pi^{b,p+1}$ is defined by the expression

$$
\begin{aligned}
\Pi^{b,p+1} &= M(t_{p+1}, x_b) - M(t_p, x_b)\\
&\quad + \sum_{j=1}^{p}[M(t_{p-1-j}, x_b) - M(t_{p-j}, x_b)]\mathbf{q}_j^{p+1}\\
&\quad - \frac{1}{2}\left(\frac{M(t_{p+1}, x_{b+1}) - M(t_{p+1}, x_{b-1})}{2a} + \frac{M(t_p, x_{b+1}) - M(t_p, x_{b-1})}{2a}\right)\\
&\quad - \left(\frac{1}{2}(M(t_{p+1}, x_b) + M(t_p, x_b))\right)(\mathbb{S}^{b,p+1} + \mathbb{S}^{b,p})\\
&\quad + \left(\left[\frac{1}{4}(M(t_{p+1}, x_b) + M(t_p, x_b))\right](\mathbb{S}^{b,p+1} + \mathbb{S}^{b,p})\right)(M(t_{p+1}, x_b) + M(t_p, x_b)).
\end{aligned}
$$

Using all the four systems (23), (24), (26), and (28) leads to

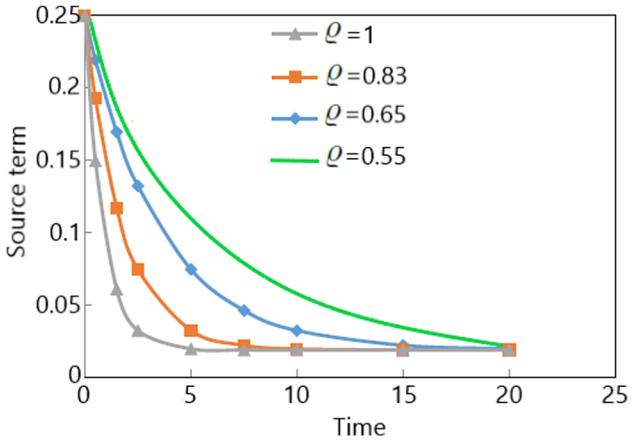

Figure 4: Variation of the source term $\mathbb{S}$ as time t is taken from 0 to 20.

$$\Pi^{b,p+1} \leq \gamma(a^2\nu^{\varrho} + 2\nu^{1+\varrho}), \tag{29}$$

with the constant γ, which is strictly positive and real.

Interpreting Inequality (29), it is clear that the growth of $\Pi^{b,p+1}$ is dependent on how $a^2\nu^{\varrho} + 2\nu^{1+\varrho}$ grows also. It means that both $\Pi^{b,p+1}$ and $a^2\nu^{\varrho} + 2\nu^{1+\varrho}$ grow at a similar and comparative pace. Additional information, concepts, and methods related to error analysis in generalized fractional processes can be found in previous studies [22,23] and references therein. From the aforementioned observation, we prove the following convergence result:

Proposition 2.2. *The approximation scheme based on Crank–Nicholson approach described in* Section 2 *and used to approximate the solution for the mass transfer Systems* (5)–(7) *converges, and we have the following inequality condition*:

$$\|\Psi^{p+1}\|_{\infty} \leq \gamma(a^2\nu^{\varrho} + 2\nu^{1+\varrho})(\mathbf{E}_j^{b,p+1})^{-1},$$

with $1 \leq j \leq p$ *and* $p = 0, 1, \ldots, \mathbf{n} - 1$ *and* $\|\Psi^{p}\|_{\infty} = \max_{1\leq b\leq \mathbf{m}-1}|\Psi^{b,p}|$ *and* $\gamma > 0$ *representing a constant.*

The theoretical analysis performed in the two sections above allows us to understand the importance of using the Crank–Nicholson method described in Section 2 in the solvability of the mass transfer Systems (5)–(7). We know now that the scheme is stable and is convergent. These two conditions are crucial to guarantee the well-posedness of the method involved in the system's solvability. The convergence condition given Proposition 2.2, for instance, is very important for the full and thorough investigation, interpretation, and explanation of the mass transfer phenomena, which is under study in this article.

2.3 Numerical representation: Multi-grouping dynamics

From the previous analysis, results and proofs, it is now clear that the scheme chosen to solve the mass transfer Systems (5)–(7) is stable and converges. This allows the presentation of some numerical representations in order to analyze the behavior of the approximated solutions.

We can refer to Table 1 for related parameters' value. The source term plays a non-negligible role in the multi-grouping dynamic, and its trajectory with regard to the time t is shown in Figure 4.

Let us associate with the system the following initial and boundary conditions, respectively, given as

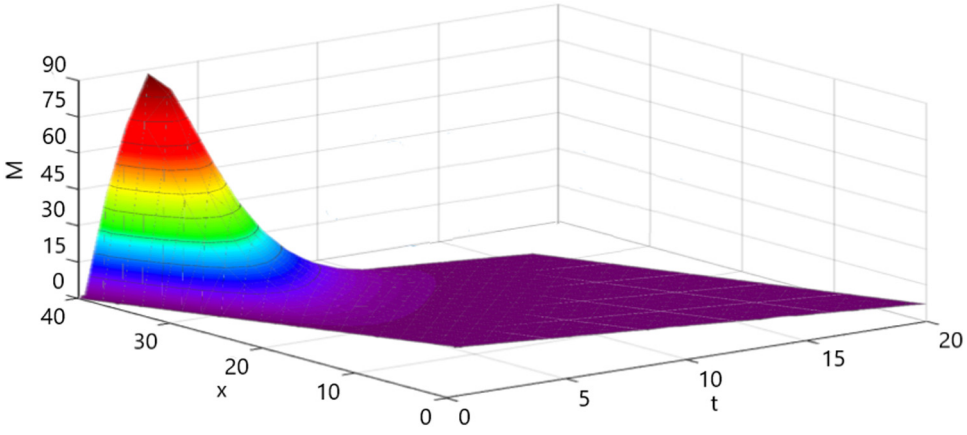

Figure 5: Spatial evolutive dynamics of the mass involved in the transfer process, when $\varrho = 1$, within the x-space interval $[0, 40]$ as time t varies from 0 to 20. It shows only one major mass grouping arising mostly in the interval $30 \leq x \leq 40$, for $t \in [0, 4]$. There is a relatively uniform and flat evolution elsewhere in the space.

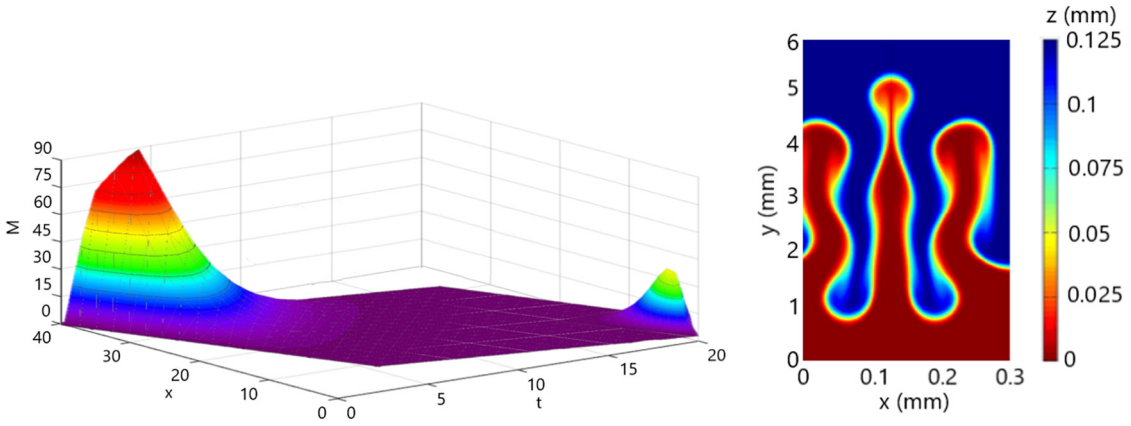

Figure 6: (Left) Spatial evolutive dynamics of the mass involved in the transfer process, when $\varrho = 0.83$, within the x-space interval $[0, 40]$ as time t varies from 0 to 20. It shows two major mass grouping arising mostly in the interval $30 \le x \le 40$, for $t \in [0, 4]$ and in the interval $2 \le x \le 8$, for $t \in [17, 19]$. There is a relatively uniform and flat evolution elsewhere in the space. (Right) Related spatial distribution.

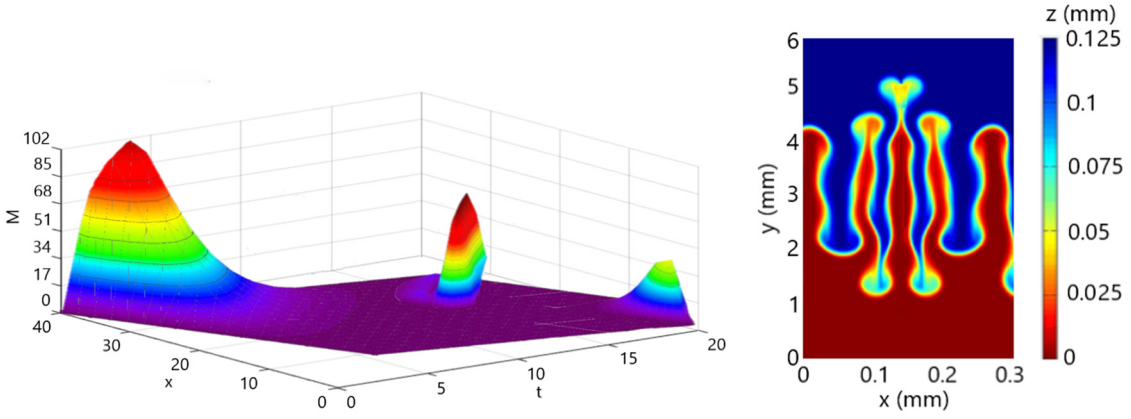

Figure 7: (Left) Spatial evolutive dynamics of the mass involved in the transfer process, when $\varrho = 0.65$, within the x-space interval $[0, 40]$ as time t varies from 0 to 20. It shows three major mass groupings arising mostly in the interval $30 \le x \le 40$, for $t \in [0, 4]$ then, in the interval $16 \le x \le 19$, for $t \in [13, 14]$, and in the interval $2 \le x \le 8$, for $t \in [17, 19]$. There is a relatively uniform and flat evolution elsewhere in the space. (Right) Related spatial distribution.

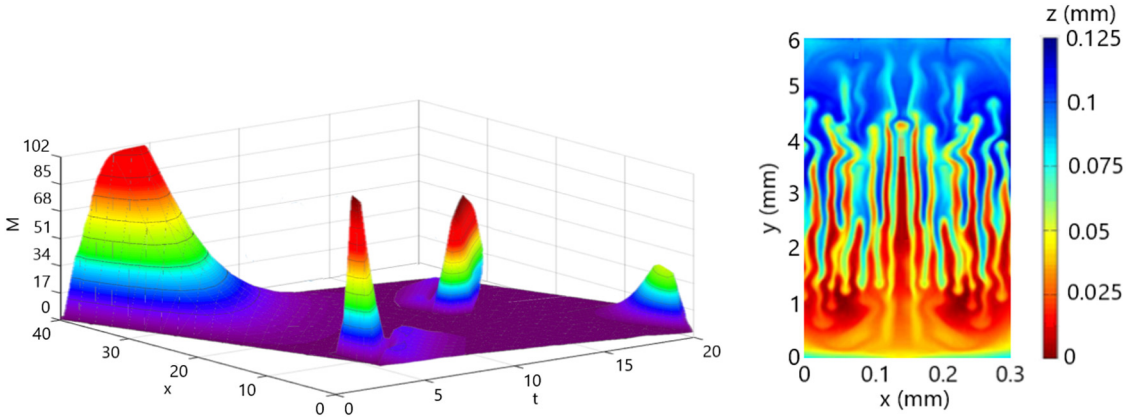

Figure 8: (Left) Spatial evolutive dynamics of the mass involved in the transfer process, when $\varrho = 0.55$, within the x-space interval $[0, 40]$ as time t varies from 0 to 20. It shows four major mass grouping arising mostly in the same areas as in Figure 7 and also in the interval $9 \le x \le 11$, for $t \in [6, 10]$. There is a relatively uniform and flat evolution elsewhere in the space. (Right) Related spatial distribution.

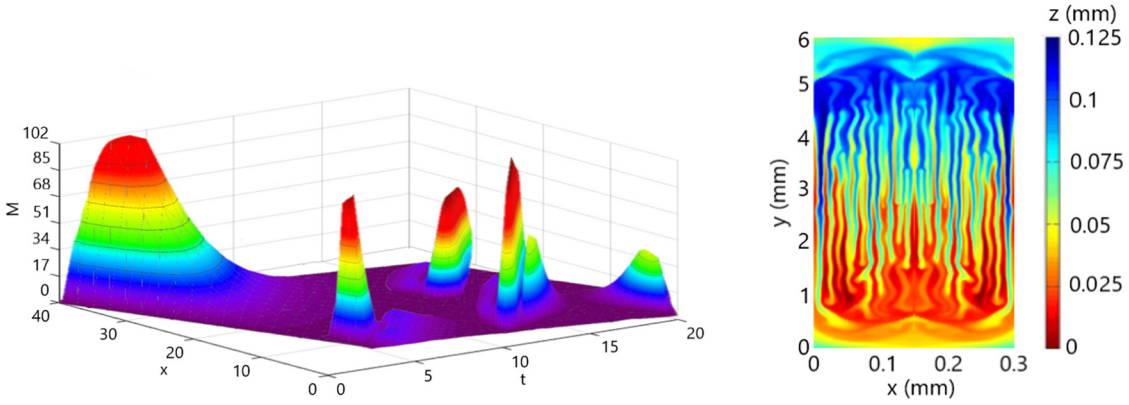

Figure 9: (Left) Spatial evolutive dynamics of the mass involved in the transfer process, when $\varrho = 0.40$, within the x-space interval $[0, 40]$ as time t varies from 0 to 20. It shows many major mass grouping arising mostly in the same areas as in Figure 8 and also in other areas scattered here and there. (Right) Related spatial distribution.

$$M(0, x) = \phi(x) = \frac{x^3}{3} \tag{30}$$

and

$$M(t, 0) = \frac{t}{3}, \quad M(t, \mathbf{L}) = \frac{\cosh t}{3}, \tag{31}$$

and choose $\mathbf{L} = 40$. Numerical simulations representing the physical evolution of mass during the transfer process are depicted in Figure 5–9. In Figure 5, for instance, we have the physical evolution of mass during the transfer taken at different time t ($0 \le t \le 20$) and space x ($0 \le x \le 40$) for $\varrho = 1$. A single major mass grouping is observed only at the beginning ($t \in [0, 4]$) in the interval $30 \le x \le 40$, before dissipating later on and becoming relatively uniform and flat. In Figure 6, for $\varrho = 0.83$, we have two major mass groupings that are observed mostly in the interval $30 \le x \le 40$, for $t \in [0, 4]$ and in the interval $2 \le x \le 8$, for $t \in [17, 19]$. The evolution is uniform elsewhere in the space.

In Figure 7, for $\varrho = 0.65$, we have three major mass groupings that are observed at different average times at the beginning ($t = 2$), the middle ($t \simeq 12$), and toward the end ($t \simeq 19$.). Hence, the groupings are mostly in the interval $30 \le x \le 40$, for $t \in [0, 4]$, then, in the interval $16 \le x \le 19$, for $t \in [13, 14]$ and in the interval $2 \le x \le 8$, for $t \in [17, 19]$. The evolution is shown to be uniform elsewhere in the space. Similar observation is made in Figure 8, plotted for $\varrho = 0.55$ and where there are four major mass groupings arising mostly in the same areas as in Figure 7 and also in the interval $9 \le x \le 11$, for $t \in [6, 10]$. There is a relatively uniform and flat evolution elsewhere in the space. Finally, in Figure 9, plotted for $\varrho = 0.40$, there are many more major mass groupings that are forming during the evolution, are scattered here and there, and seem to increase as the parameter ϱ decreases. The mass transfer process appears to be highly dynamic and active in Figures 8 and 9 compared to Figures 5 and 6, meaning that the parameter ϱ is playing an important role in terms of controlling the quantity of mass being transferred. There is in reality an increasing mass (CO_2) accumulation with respect to the parameter ϱ, as shown in Figure 10.

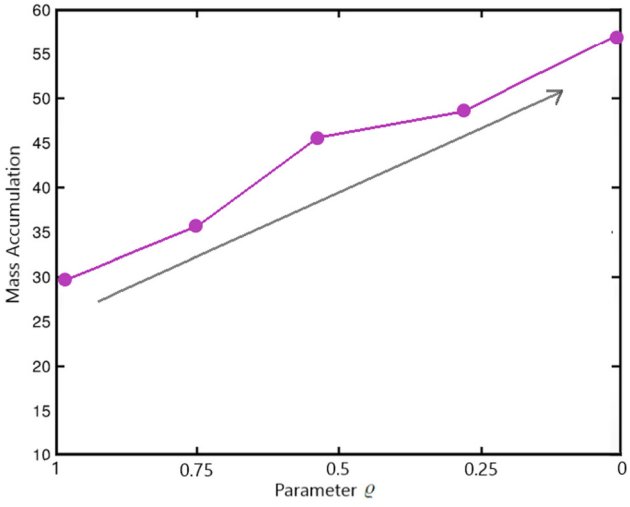

Figure 10: Increasing mass accumulation with respect to the parameter ϱ.

3 Conclusion

We have investigated the solvability of a mathematical model describing the mass transport process in nature and where additional perturbation parameters have been considered. After addressing the stability of the model, its convergence analysis has also been done in order to assess

its efficiency and perform some numerical simulations. The results obtained have shown that the model's dynamic is characterized by many accumulation zones where the mass, of CO_2, for instance, can accumulate in an increasing way. The observed increasing accumulation appears to be dependent on the model's parameter, namely, the order. The results exposed in this article are also important as they prove that the model can be used to control the way mass (of CO_2, for instance) can be stored in this growingly perturbed environment that is changing the way we live. This observation is even more crucial especially nowadays where the emission of CO_2 in the atmosphere is classified as the prime cause of climate change touching the whole globe and causing catastrophes and calamities all over the planet.

Funding information: The authors state no funding involved.

Author contributions: Emile Franc Doungmo Goufo: conceptualization, methodology, software, writing – part of original draft, formal analysis. Amos Kubeka: methodology, writing – part of original draft, simulations, reading, correcting, editing. All authors have accepted responsibility for the entire content of this manuscript and approved its submission.

Conflict of interest: The authors state no conflict of interest.

References

[1] WorldAtlas. How Is Climate Change Impacting The Water Cycle? https://wwwworldatlascom/the-water-cyclehtml. [accessed 11 Oct, 2022].
[2] Li J, Hou Y, Wang P, Yang B. A review of carbon capture and storage project investment and operational decision-making based on bibliometrics. Energies. 2018;12(1):23.
[3] Skočilasová B, Skočilas J, Soukup J. Forced convection and heat transfer around a bounded cylinder. In: MATEC Web of Conferences. vol. 157. EDP Sciences; 2018. p. 02045.
[4] Li BQ. Discontinuous finite elements in fluid dynamics and heat transfer. Springer Science & Business Media; 2005.
[5] Kilbas AAA, Srivastava HM, Trujillo JJ. Theory and applications of fractional differential equations. vol. 204. Elsevier Science; 2006.
[6] Zaccone A, Wu H, Gentili D, Morbidelli M. Theory of activated-rate processes under shear with application to shear-induced aggregation of colloids. Phys Rev E. 2009;80(5):051404.
[7] Caputo M, Fabrizio M. A new definition of fractional derivative without singular kernel. Progr Fract Differ Appl. 2015;1(2):1–13.
[8] Losada J, Nieto JJ. Properties of a new fractional derivative without singular kernel. Progr Fract Differ Appl. 2015;1(2):87–92.
[9] Atangana A. On the stability and convergence of the time-fractional variable order telegraph equation. J Comput Phys. 2015;293:104–14.
[10] Lin R, Liu F, Anh V, Turner I. Stability and convergence of a new explicit finite-difference approximation for the variable-order nonlinear fractional diffusion equation. Appl Math Comput. 2009;212(2):435–45.
[11] Zhuang P, Liu F, Anh V, Turner I. Numerical methods for the variable-order fractional advection-diffusion equation with a nonlinear source term. SIAM J Numer Anal. 2009;47(3):1760–81.
[12] Goufo EFD, Pene MK, Mugisha S. Stability analysis of epidemic models of Ebola hemorrhagic fever with non-linear transmission. J Nonlinear Sci Appl. 2016;9(6):4191–205.
[13] Chen CM, Liu F, Turner I, Anh V. A Fourier method for the fractional diffusion equation describing sub-diffusion. J Comput Phys. 2007;227(2):886–97.
[14] Meerschaert MM, Tadjeran C. Finite difference approximations for fractional advection-dispersion flow equations. J Comput Appl Math. 2004;172(1):65–77.
[15] Tadjeran C, Meerschaert MM, Scheffler HP. A second-order accurate numerical approximation for the fractional diffusion equation. J Comput Phys. 2006;213(1):205–13.
[16] Liu Y, Fang Z, Li H, He S. A mixed finite element method for a time-fractional fourth-order partial differential equation. Appl Math Comput. 2014;243:703–17.
[17] Zhang Y. A finite difference method for fractional partial differential equation. Appl Math Comput. 2009;215(2):524–9.
[18] Yuste SB, Acedo L. An explicit finite difference method and a new von Neumann-type stability analysis for fractional diffusion equations. SIAM J Numer Anal. 2005;42(5):1862–74.
[19] Hanert E. On the numerical solution of space-time fractional diffusion models. Comput Fluids. 2011;46(1):33–9.
[20] Podlubny I, Chechkin A, Skovranek T, Chen Y, Jara BMV. Matrix approach to discrete fractional calculus II: partial fractional differential equations. J Comput Phys. 2009;228(8):3137–53.
[21] Crank J, Nicolson P. A practical method for numerical evaluation of solutions of partial differential equations of the heat-conduction type. In: Mathematical Proceedings of the Cambridge Philosophical Society, vol. 43, No. 1, Cambridge: Cambridge University Press; 1947, pp. 50–67.
[22] Diethelm K, Ford NJ, Freed AD. Detailed error analysis for a fractional Adams method. Numer Alg. 2004;36(1):31–52.
[23] Li C, Tao C. On the fractional Adams method. Comput Math Appl. 2009;58(8):1573–88.